Hindawi Publishing Corporation
Advances in Condensed Matter Physics
Volume 2009, Article ID 327605, 8 pages
doi:10.1155/2009/327605

Research Article

Optical Properties of $LiIn_{(1-x)}Tm_x(WO_4)_2$ Blue Phosphor

Mourad Derbal,[1,2] Lakhdar Guerbous,[3] Ouadjaout Djamel,[4] Chaminade Jean Pierre,[2] and Mohyddine Kadi-Hanifi[5]

[1] *LASICOM, Saad Dahlab University, BP 270, Route de Soumaa, 09000, Blida, Algeria*
[2] *ICMCB, Bordeaux I University, 87 avenue A. Schweitzer, 33608 Pessac, France*
[3] *Laser Department, Nuclear Research Center of Algiers-CRNA, 2 Building Frantz Fanon, B.P 399 Alger 16000, Algeria*
[4] *UDTS, 2 Building Frantz Fanon, BP. 140 Alger-7 Merveilles, 16200 Alger, Algeria*
[5] *LSS, Université des Sciences et de la Technologie Houari Boumediene, BP 32, EL ALIA 16111 BAB EZZOUAR ALGER.USTHB, Faculté de Physique, Alger, Algeria*

Correspondence should be addressed to Lakhdar Guerbous, guerbous@yahoo.fr

Received 28 July 2009; Revised 8 November 2009; Accepted 30 November 2009

Recommended by David Huber

$LiIn_{1-x}Tm_x(WO_4)_2$ (x = 0, 0.5, 1, 5, and 10 at.%) polycrystalline powders blue phosphors were prepared via the classical solid-state reaction method. X-ray diffraction (XRD), scanning electron microscope (SEM), photoluminescence excitation, and emission spectra were used to characterize $LiIn_{1-x}Tm_x(WO_4)_2$ phosphors. By analyzing the excitation and emission spectra of $LiIn_{1-x}Tm_x(WO_4)_2$ samples, the result indicates that there exists the energy transfer only from the WO_4^{2-} group to the $^1G_4$ energy level of Tm^{3+} ion. On the other hand, the influence of the thulium concentration on the blue emission transition $^1D_2 \rightarrow {}^3F_4$ and $^1G_4 \rightarrow {}^3H_6$ and the emission of WO_4^{2-} group are investigated.

1. Introduction

Rare-earth ions-doped double tungstates have attracted a great deal of interest in recent years, due to their efficient radiative emissions in the visible and mid-infrared spectral regions [1–5]. These emissions are suitable for developing potential applications such as active media in solid-state lasers [6–10] and inorganic scintillation materials thanks to their high density (7.46 (g/cm^3) for $LiIn(W_4)_2$) and to the fast emission of the $(WO_4)^{-2}$ tungstate group [11, 12].

Trivalent thulium could be an attractive activator ion exhibiting the suitable strong absorption band for the commercial GaAlAs laser diodes pumping around 800 nm, corresponding to the $^3H_6 \rightarrow {}^3H_4$ transition. Especially, the 2 μm region meets a great interest in many fields and applications like optical communications, medical equipment, and remote sensing [13–15].

Furthermore, Tm-doped materials, such as YLF, YAG, and NYW, generate blue laser radiation through the up-conversion of infrared radiation into visible radiation [16].

Especially, solid-state blue light sources are desirable for several applications, including high-density optical storage and colour displays, but, it has been difficult to find a suitable blue phosphor. Tm^{3+} ion is among activators which can be used for obtaining blue emission corresponding to its $^1D_2 \rightarrow {}^3F_4$ and $^1G_4 \rightarrow {}^3H_6$ transitions [17].

$LiIn(WO_4)_2$ belongs to the large family of inorganic compounds with the general formula $M^IM^{III}(M^{VI}O_4)_2$, where M^I = alkali metal, or monovalent transition metal ions; M^{III} = Al, In, Sc, Cr, Bi, Fe, rare earth ion, and M^{VI} = Mo, W. These materials may crystallize in a wide number of structures, which may be related as originating from either the structure of scheelite ($CaWO_4$), with isolated $M^{VI}O_4$ tetrahedra, or the structure of wolframite ($FeWO_4$), with octahedral coordination of M^{VI} Atoms [18, 19].

Due to the useful laser transitions of Tm^{3+} at both the visible and infrared frequencies, much attention has been paid in identifying optimal host crystals for these ions. In fact, the Tm^{3+} ions have demonstrated laser action in different spectral ranges in a wide variety of host crystals

pumped with flash lamp, ion laser, or diode laser. However, as far as we know, there are no reports concerning thulium-doped monoclinic $LiIn(WO_4)_2$ host.

In paper, polycrystalline powders of Tm^{3+} : $LiIn(WO_4)_2$ were prepared using the classical solid-phase chemical reaction. First results of the structural and spectroscopic investigations of this material are presented. FTIR and photoluminescence spectra, especially charge transfer bands observed in the UV region, are analyzed. We also investigate the dependence of the blue emission intensity versus Tm^{3+} ions concentration in the material, under resonant $^1D_2$ level excitation ($\lambda_{ex} = 360$ nm) and W-O ligand-to-metal charge transfer band energy.

2. Experimental Procedures

2.1. Powder Preparation. Polycrystalline powders of $LiIn_{1-x}Tm_x(WO_4)_2$, where x is the Tm^{3+} ions concentration ($x = 0$, 0.5, 1, 5, and 10 at.%), are synthesized by means of classical solid-state reaction according to the following reaction:

$$\frac{1}{2}Li_2CO_3 + \frac{(1-x)}{2}In_2O_3 + \frac{1}{2}x\ Tm_2O_3 + 2\ WO_3 \longrightarrow LiIn_{1-x}Tm_x(WO_4)_2 + \frac{1}{2}\ CO_2\uparrow. \quad (1)$$

Stoichiometric amounts of the starting materials: Li_2CO_3 (Alfa Aesar, 99.998%), In_2O_3 (CERAC, 99.99%), WO_3 (Ventron, 99.7%), and Tm_2O_3 (Aldrich Chemical Cie, 99.99%), of analytical grade purity, weighed in suitable molar proportions (Mettler Toledo PR 2003 balance) were ground and mixed manually in an agate mortar. The mixture was placed in a Pt crucible, and then heated in an electrical furnace. The mixtures were carefully ground, mixed, and then calcined in air at 700°C for 15 hours. After regrinding, the samples were finally calcined in air at 950°C fot 15 hours.

The samples were gradually cooled down to room temperature, weighed, ground, and analyzed using XRD method. After the final heating cycle, the samples were examined by Differential Thermal Analysis (DTA).

2.2. Characterization Techniques. Phase purity and crystal structure of the synthesized compounds were determined by X-ray diffraction analysis (XRD). Powder XRD patterns were collected at ambient temperature with a Philips PW1820 diffractometer (Cu Kα radiation, $\lambda = 1.54056$ Å, $2\theta = 10$–50°). Lattice parameters were refined from XRD data recorded on powder samples, using the WinPLOTR-2006 program (LLB Saclay- LCSIM Rennes).

The morphology and microstructure were characterized by scanning electron microscope (SEM, Philips XL-30). IR spectra at 300 K were recorded with Thermo-Nicolet "Nexus"-670 FT-IR spectrophotometer, yielding a spectral resolution of 4 cm^{-1}. The samples were mixed with KBr with a sample/KBr weight ratio of ~1/100 and compressed to give self-supporting pellets. For each sample 128 scans were recorded.

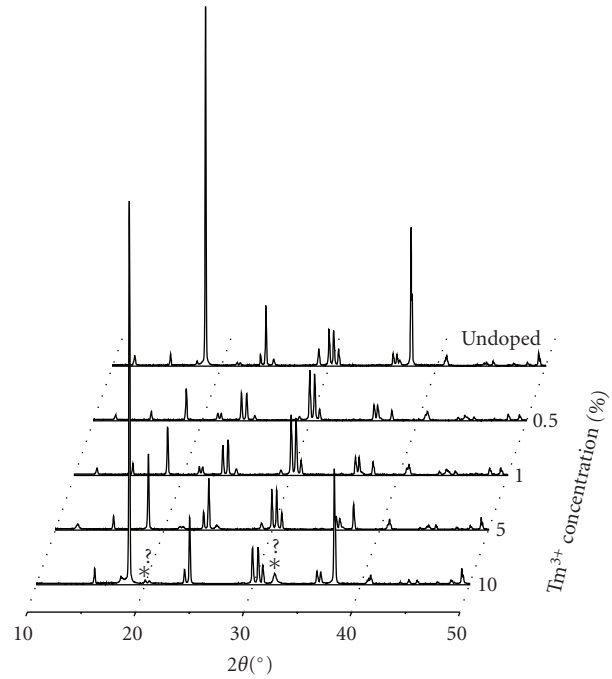

FIGURE 1: XRD patterns of $LiIn_{1-x}Tm_x(WO_4)_2$ ($x = 0$, 0.5, 1, 5, and 10 at.%).

Room temperature diffuse absorption measurements were performed using a CARY 500 UV-VIS-NIR spectrophotometer in the range 250–1350 nm, with a resolution of 0.3 nm in the UV-VIS wavelength region and 1 nm in the NIR. This spectrometer is equipped with an integrating sphere accessory coated with PTFE (Poly Tetra Fluoro Ethylene) white material. The diffuse reflectance measurements were converted into absorption (arbitrary units) using the Kubelka-Munk function ($f(R_\infty) = K/S_{sca} = (1-R_\infty)^2/2R_\infty$) [20],where K is the absorption, R_∞ is the diffuse reflectance rate and S_{sca} is the diffusion factor.

Perkin-Elmer LS-50B spectrofluorimeter was used for room temperature steady-state luminescence measurements. For recording the excitation and the emission spectra, unpolarized light from the Xenon lamp (150 W) was used. The spectra were collected at right angle using a special sample holder. The values of the slit widths for the excitation and emission monochromators were set at spectral resolutions of 2.5 nm and 2.5 nm, respectively. The limit range is between 200 to 900 nm.

3. Results and Discussion

3.1. Crystal Structure of the Host. Monoclinic $LiIn(WO_4)_2$ crystallizes in the wolframite structure and is isostructural to $LiFe(WO_4)_2$ with the space group $C2/c = C^6_{2h}$ and $Z = 4$. Accordingly to the $C2/c$ space group, the Li and In ions occupy the nonequivalent positions on the 2 and 2_1 axes [18, 19, 21, 22]. The unit-cell dimensions at room temperature are, $a = 9.58$ Å, $b = 11.59$ Å, $c = 4.956$ Å, and

Table 1: Calculated unit cell parameters for various thulium concentrations.

Tm at. (%)	a (Å)	b (Å)	c (Å)	β (∘)
0	9.580	11.590	4.956	91.078
0.5	9.579	11.581	4.955	91.120
1	9.585	11.584	4.957	91.128
5	9.587	11.582	4.956	91.135

$\beta = 91.078^\circ$. The crystal is built up of $(WO_6)^{6-}$ octahedron connected to each other by means of common edges, forming $(WO_4)^{2-}$ zigzag chains along the *c*-direction. Lithium and indium atoms occupy both octahedral sites and constitute $(LiO_4)^{7-}$ and $(In\,O_4)^{5-}$ chains ordered in *a* and *b* directions. Consequently, In^{3+} octahedrons share common edges in the chain. This type of structure is encountered in compounds where difference of ionic radii of M^+ and M^{3+} is low ($r_{Li}{}^+ = 0.76\,Å$, $r_{In}{}^{3+} = 0.80\,Å$ [23]).

The XRD patterns of $LiIn_{1-x}Tm_x(WO_4)_2$ ($x = 0$, 0.5, 5, and 10 at.%), are shown on Figure 1, from which we can see that for $x = 0$, 0.5, and 5 at.% all the diffraction peaks of each sample can be indexed to the phase of monoclinic $LiIn(WO_4)_2$ (pdf code 00-049-0963). For the sample which $x = 10$ at.%, there are two ones additional peaks with weaker intensity at the diffraction angles: $2\theta = 32^\circ$, 20.4° of non identified phase.

The knowledge of the unit cell variation with Tm^{3+} doping is important, for example, for epitaxial growth of doped layers on undoped substrates. In Table 1, we present the optimized unit-cell parameters deduced from the previous XRD analysis for all concentration except 10%. The unit-cell parameters *a*, *c*, *b,* and β remain basically constant when the doping concentration of Tm^{3+} increases. For $x = 10$ at %, at that time no interpretation can be done. Growth of single crystals will be accomplished in order to resolve this problem.

Figures 2(a) and 2(b) show the DTA curves of pure $LiIn(WO_4)_2$ sample corresponding to the melting and crystallization process, respectively. A single sharp endothermic peak is observed at around 1093°C. This peak exhibits the characteristics of a first-order phase transition which corresponds to a solid-liquid phase change, identified as the melting point. DTA analysis indicates that the fusion of the product is clearly congruent, and then one can attempt to pull a single crystal by the Czochralski technique.

3.2. Surface Morphological Analysis. In order to observe the grain morphology of the prepared powders with varying the Tm^{3+} concentration, we have taken for each sample some scanning electron microscope (SEM) images. For all studied Tm^{3+} concentrations, the SEM picture (Figure 3) exhibits particles with the same and definite shapes and sizes. The distribution of these particles is random and overlaps each other. The typical crystalline grain size is estimated to be in the range 0.5–2.0 micrometers.

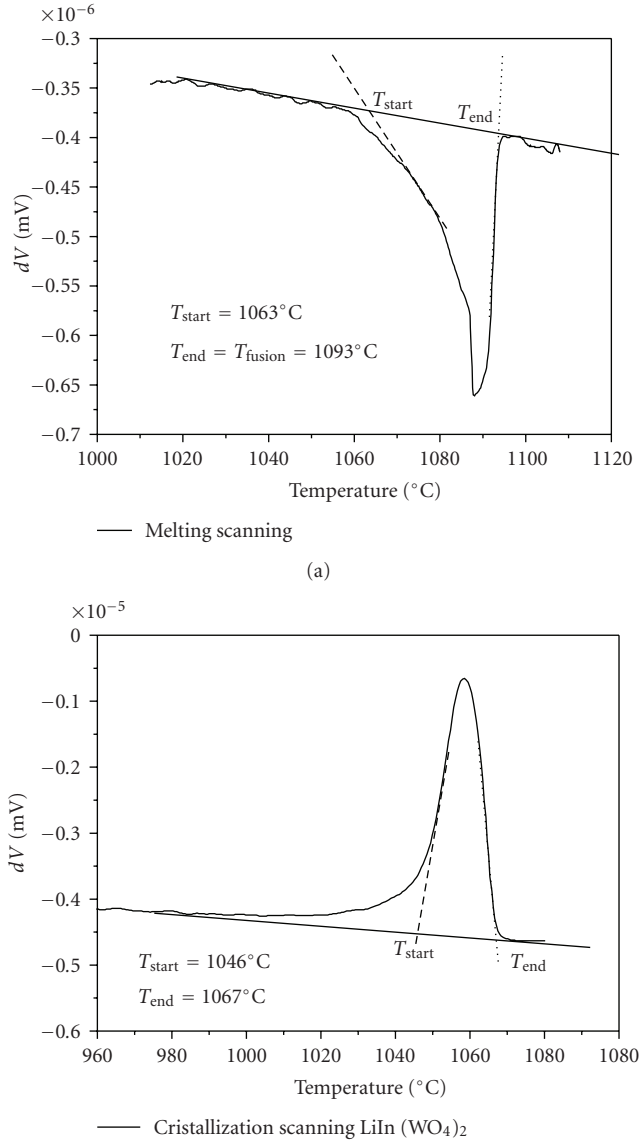

Figure 2: DTA curves of pure $LiIn(WO_4)_2$ during the (a) heating cycle and (b) cooling cycle.

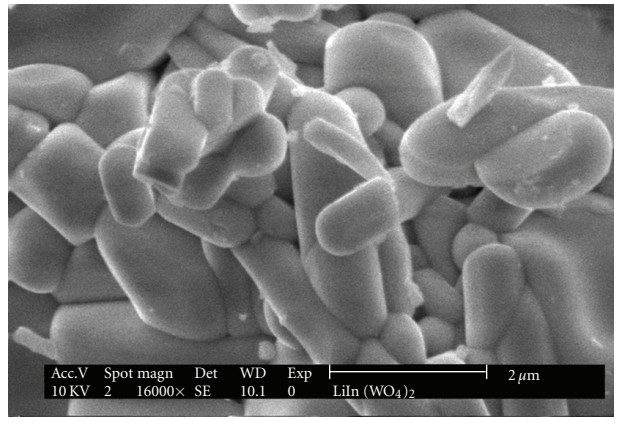

Figure 3: SEM micrograph of $LiIn_{1-x}Tm_x(WO_4)_2$.

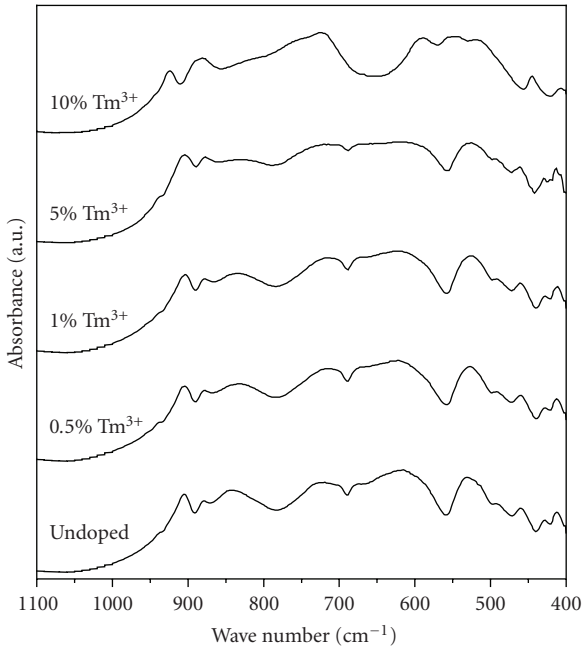

Figure 4: Room temperature FTIR spectra of $LiIn_{1-x}Tm_x(WO_4)_2$ (x = 0, 0.5, 1, 5, and 10 at.%).

3.3. Infrared Spectroscopy. Figure 4 shows the room temperature Infrared spectra of $LiIn_{1-x}Tm_x(WO_4)_2$ samples (x = 0, 0.5, 1, 5, and 10 at.%). The spectra exhibits a number of broad absorption bands, particularly in the range 400–1100 cm^{-1}. These bands are assigned to the vibration modes of WO_6 groups. These results showed that the bands in the 940–750 cm^{-1} region can be attributed to symmetric and asymmetric stretching vibrations of the terminal (short) W-O bonds [22]. Stretching vibrations of the longer W-O bonds, which take part in the formation of the ($W^O{}_OW$) bridges, were observed in the 460–725 cm^{-1} region. In the 407–445 cm^{-1} region lie the bending vibrations of the W-O bonds. These attributions are in good agreement with the previous works of Maczka [22] and Fomichev [24]. However we note that a change appears in the 785–560 cm^{-1} region for x = 10%. This is probably due to the phase change as mentioned above.

3.4. Optical Absorption. The diffuse absoption spectra of $LiIn(WO_4)_2$ doped with different concentrations of Tm^{3+} are shown in Figure 5(a). They are recorded at room temperature, in the visible and near infrared regions. One can clearly distinguish four groups of peaks which can be assigned to the intraconfigurationnal $4f^{12}$–$4f^{12}$ absorption transitions of Tm^{3+} from the ground state $^3H_6$, to the $^3H_5$ (~1200 nm), $^3H_4$ (~800 nm), $^3F_3$-$^3F_2$ (~700 nm), and $^1G_4$ (~470 nm) excited states. The intensity of these peaks increases with increasing concentration of Tm^{3+} ions. In the UV region (Figure 5(b)), the spectra present a large band located between 280 and 345 nm and attributed to the W-O charge transfer. This band is very intense compared with the peaks observed in the visible and near infrared regions.

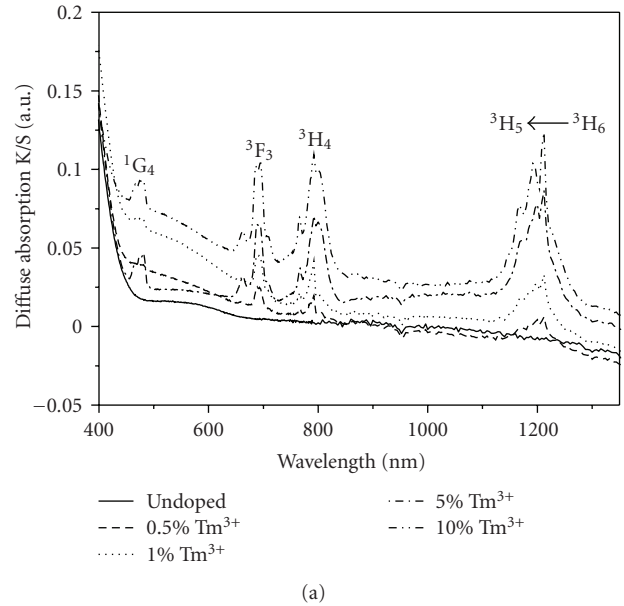

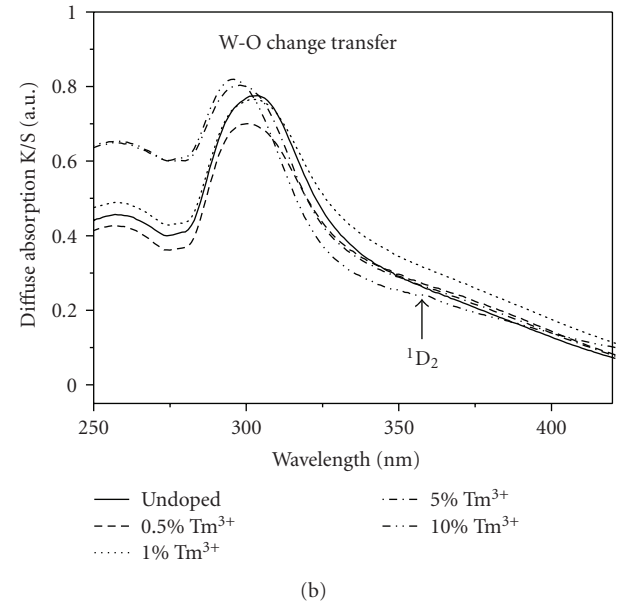

Figure 5: Diffuse absorption spectra $LiIn_{1-x}Tm_x(WO_4)_2$ (x = 0, 0.5, 1, 5, and 10 at.%): (a) visible and (b) UV regions.

3.5. Photoluminescence. Figure 6(a) shows the room temperature emission spectra of $LiIn_{1-x}Tm_x(WO_4)_2$ (x = 0, 0.5, 5, and 10 at.%), under 360 nm excitation wavelength (corresponding to the $^3H_6 \rightarrow {}^1D_2$ excitation transition). For all the Tm^{3+} concentration, the extended emission spectra between 370 and 900 nm are the same and exhibit two blue emission peaks lying between 435 nm and 455 nm. The maximum of these two bands are centered at 440 and 448 nm.

Referring on the energy level positions in the literature, Pujol et al. [25], have investigated the spectroscopic properties of Tm^{3+}-doped $KYb(WO_4)_2$ single crystals.

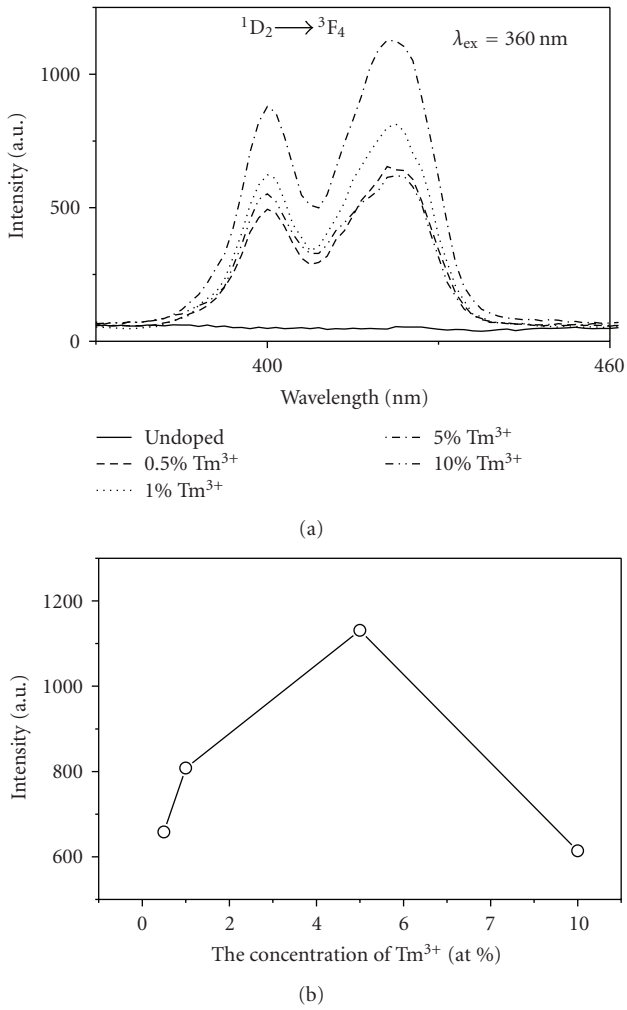

Figure 6: (a) Room temperature emission spectra of $LiIn_{1-x}Tm_x(WO_4)_2$ (x = 0, 0.5, 1, 5, and 10 at.%), excited at 360 nm wavelength. (b) Integrated emission intensity of $^1D_2 \rightarrow {}^3F_4$ transition (447 nm) in $LiIn(WO_4)_2$ as a function of Tm^{3+} concentration.

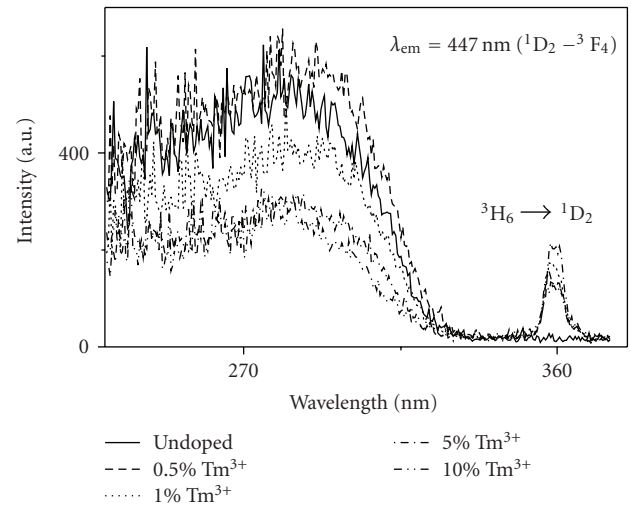

Figure 7: Room temperature excitation spectra of $LiIn_{1-x}Tm_x(WO_4)_2$(x = 0, 0.5, 1, 5, and 10 at.%), monitoring 447 nm emission wavelength ($^1D_2 \rightarrow {}^3F_4$ transition).

Therefore, these two peaks are originating from the intra-configurational $4f^{12}$–$4f^{12}$ transitions of the Tm^{3+} ions and assigned them to the $^1D_2 \rightarrow {}^3F_4$ emission transition.

By changing the concentration of Tm^{3+}ion in $LiIn(WO_4)_2$, we determine the optimum of compositions with the highest emission intensity. In the emission spectra, the peaks positions did not change as the Tm^{3+} concentration change, which indicate that the crystal structure of Tm^{3+}-doped $LiIn(WO_4)_2$ does not change. It is well known that the emission intensity increases with the activator ions concentration and at defined point of concentration begins to decrease. This phenomenon can be also explained by the quenching concentration phenomenon of the emission. Indeed, the increase of rare earth activator concentration induces the shortening of the RE^{3+}–RE^{3+} distance, and it is well known that if the distance of luminescent centers is short enough, energy can transfer among these luminescent centers following a great deal of nonradiative transitions, which leads to the quenching of luminescence [26]. In the other hand, the concentration behaviour of the luminescence is a complex matter, since different energy transfers (mainly cross relaxation) can be involved and several experimental parameters are involved.

The integrated PL intensity of $^1D_2 \rightarrow {}^3F_4$ peaks versus Tm content x at room temperature is shown in Figure 6(b). It shows that there is a saturation range of PL intensity with the Tm content from x = 0.5 to 5 at. %. As the Tm content x increases from 5 to 10 at %, the integrated PL intensity decreases due to the concentration quenching. For this transition, we consider x = 5 at % as the optimum concentration.

Under 360 nm excitation wavelength, for all the doped samples, the $^1G_4 \rightarrow {}^3H_6$ emission transition is not observed. It should be also noted that we did not observe this transitions even under the excitation directly of $^1G_4$ energy level.

Multiphonon-relaxation from $^1D_2$ to $^1G_4$ is improbable in view of the large energy gap (around 7000 cm^{-1}), with the maximum phonon energy of 940 cm^{-1} in $LiIn(WO_4)_2$ double tungstate (FTIR part); then, we need an important number of phonons (around 8 phonon). It is possible that the cross-relaxation process according the scheme: ($^1D_2 \rightarrow {}^3F_3$) + ($^3H_6 \rightarrow {}^3H_4$) or ($^1D_2 \rightarrow {}^3H_4$) + ($^3H_6 \rightarrow {}^3F_3$) is the most probably contributed to the relaxation of the $^1D_2$ level. The same phenomena have been observed by Macalik et al. [27] in the $KLa(WO_4)_2$ single crystal doped with Tm^{3+} ions.

Figure 7 displays the excitation spectra of $LiIn_{1-x}Tm_x(WO_4)_2$ (x = 0, 0.5, 5, and 10 at.%), recorded at room temperature in the 230–475 nm region, for 447 nm emission wavelength ($^1D_2 \rightarrow {}^3F_4$ transition). For all samples the excitation spectra show a wide and intense band centered on 285 nm. In addition, a sharp peak having weaker intensity located at 360 nm is observed. This peak is not observed for the nondoped sample and presents the same

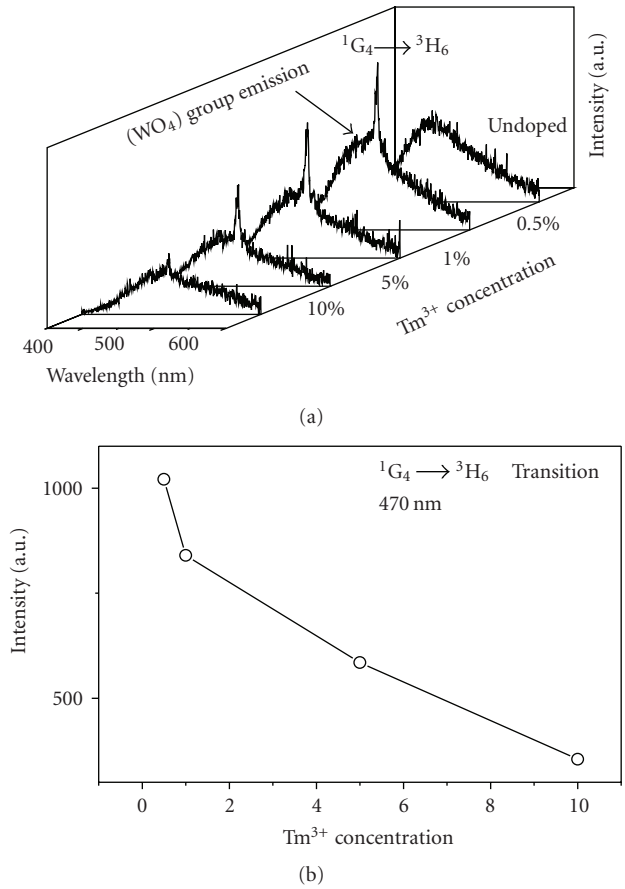

FIGURE 8: (a) Room temperature emission spectra of $LiIn_{1-x}Tm_x(WO_4)_2$ (x = 0, 0.5, 1, 5, and 10 at.%) excited at 285 nm, (b) Integrated emission intensity for $^1G_4 \rightarrow {}^3H_6$ transition (470 nm) in $LiIn(WO_4)_2$ as a function of Tm^{3+} concentration.

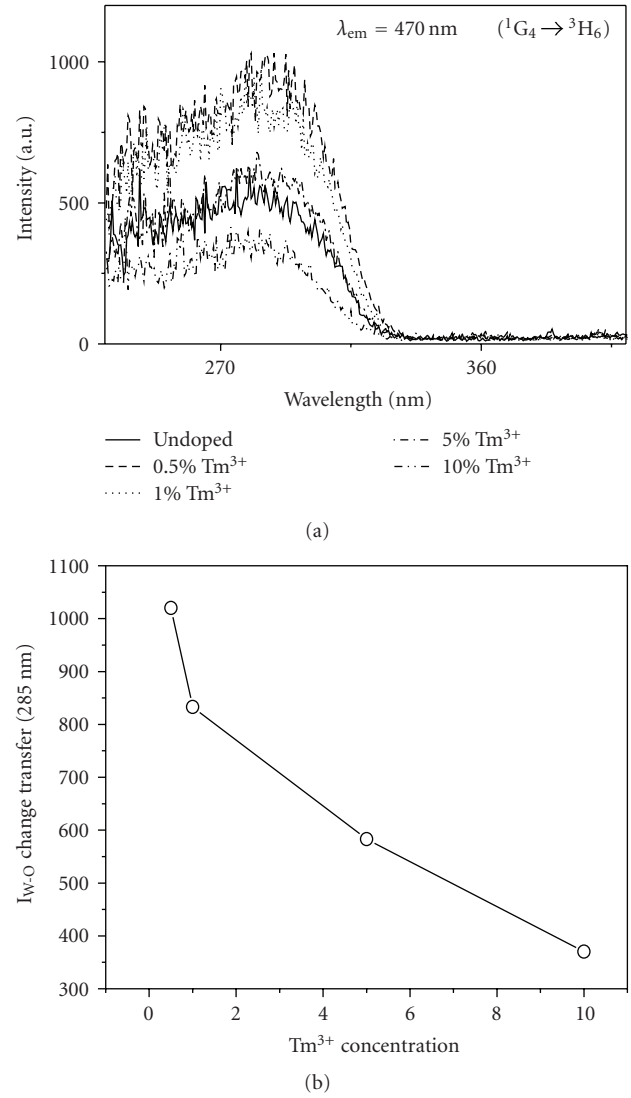

FIGURE 9: (a) Room temperature excitation spectra of $LiIn_{1-x}Tm_x(WO_4)_2$, (x = 0, 0.5, 1, and 5 at.%), monitoring 470 nm emission wavelength ($^1G_4 \rightarrow {}^3H_6$transition) (b) W-O charge transfer excitation band intensity monitoring 470 nm emission ($^1G_4 \rightarrow {}^3H_6$transition) as a function of Tm^{3+} concentration.

variation of their intensity against the Tm^{3+} concentration, identical to the emission spectra (see Figure 6(a)). Based on the energy scheme of Tm^{3+}, we have assigned this peak to the $^3H_6 \rightarrow {}^1D_2$ excitation transition. The intense band around 285 nm should be assigned to the W-O ligand-to-metal charge transfer states (LMCT) from (WO_6) units in the $LiIn(WO_4)_2$ host lattice.

Room temperature emission spectra of $LiIn_{1-x}Tm_x(WO_4)_2$ (x = 0, 0.5, 5, and 10 at.%), under the excitation wavelength of 285 nm (corresponding to the W-O ligand-to-metal charge transfer) between 400 and 600 nm, are shown on the Figure 8(a). There are two kinds of emission for all doped phosphors observed, a narrow peak at 470 nm originates from the Tm^{3+} ion transition $^1G_4 \rightarrow {}^3H_6$, and a broad-band centred around on 450 nm. This broad emission band is ascribed to the radiative decay of the regular lattice centre $(WO_4)^{-2}$ or radiative decay of excitons self-trapped (localized) on regular $(WO_4)^{-2}$ groups. Tungstate complexes are usually characterized by a broad band emission with large Stokes shift (10000 cm^{-1} (1.24 eV) to −20000 cm^{-1} (2.28 eV)) from the absorption [28].

With increasing Tm^{3+} concentration, the narrow peak intensity decreases with the increasing from 0.5 to 10 at.% (Figure 8(b)) due to the concentration quenching. The intensity of broad-band decreases also with Tm^{3+} concentration in full studied concentration region, which implies that the energy transfer from $(WO_4)^{-2}$ to Tm^{3+} increases. We believe that the optimum of compositions with the highest emission intensity for $^1G_4 \rightarrow {}^3H_6$is lower than 0.5 at.%.

On Figure 9(a), the excitation spectra of $LiIn_{1-x}Tm_x(WO_4)_2$ (x = 0, 0.5, 5, and 10 at.%), recorded at room temperature in the 230–410 nm region, for 470 nm emission wavelength ($^1G_2 \rightarrow {}^3H_4$ transition) are displayed. For all samples the excitation spectra show only a wide and intense band centered on 285 (W-O ligand-to-metal

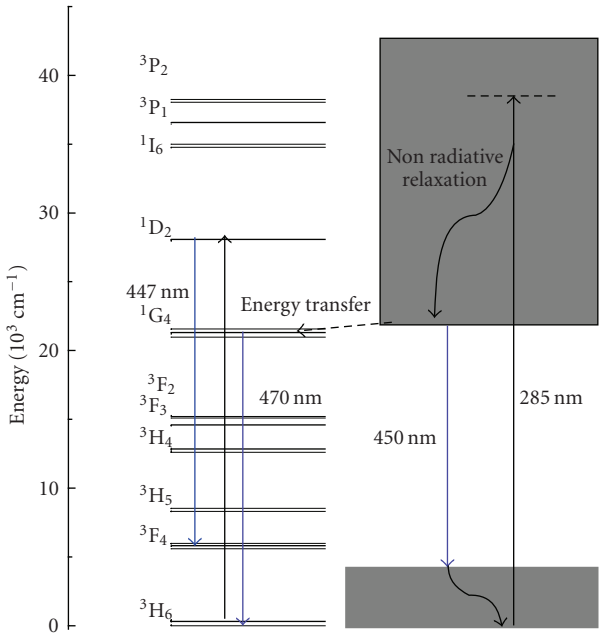

Figure 10: Energy level diagram and luminescence process mechanism of Tm^{3+} in $LiIn(WO_4)_2$.

charge transfer states). The presence of the strong absorption band of (WO_6) groups in the excitation spectrum of Tm^{3+} indicates that there exists an energy transfer from (WO_6) groups to $^1G_4$ energy level of Tm^{3+} ions in $LiIn(WO_4)_2$. The nonobservation of $^3H_6 \rightarrow {}^1D_2$ excitation transition confirms our suggestion above that there is no multiphonon relaxation between $^1D_2$ and $^1G_4$. As the Tm^{3+} concentration increases, the W-O ligand-to-metal charge transfer band intensity (285 nm) decreases as shown on Figure 9(b). This is confirming the suggestion that the increasing with the Tm^{3+} concentration, the energy transfer between $(WO_4)^{-2}$ excited state and the $^1G_4$ level increases.

No emission transition $^1D_2 \rightarrow {}^3F_4$ (447 nm) is recorded despite the existence of the W-O ligand-to-metal charge transfer band in the excitation spectrum monitoring the emission wavelength of this emission transition (see Figure 7). The existence of this band is simply due to the position of the $^1D_2 \rightarrow {}^3F_4$ emission transition wavelength (447 nm), which is very close to the emission of $(WO_4)^{-2}$ group (maximum 450 nm). Therefore, no energy transfer is occurring between W-O ligand-to-metal charge state and $^1D_2$ energy level. on Figure 10, we proposed a tentative energy level diagram and luminescence process mechanism to help in the understanding of the present spectroscopic results for Tm-doped $LiIn(WO_4)_2$.

4. Conclusion

Blue emitting $LiIn_{1-x}Tm_x(WO_4)_2$ (x = 0, 0.5, 1, 5, and 10 at.%) polycrystalline powders phosphors have been successfully synthesized by means of classical solid-phase reaction by means of classical solid-phase reaction. For all Tm^{3+} concentrations, optical spectra recorded at room temperature exhibit the absorption of $^{2S+1}L_J$ energy levels of Tm^{3+} as well as the intrinsic W-O charge transfer bands. Blue intraconfigurationally emissions transitions $^1D_2 \rightarrow {}^3F_4$ and $^1G_4 \rightarrow {}^3H_6$ of Tm^{3+} are observed. Optimum concentration quenching for the $^1D_2 \rightarrow {}^3F_4$ transition appears to be about 5 at % Tm^{3+}, whereas the $^1G_4 \rightarrow {}^3H_6$ transition will probably be optimum for a concentration less than 0.5 at.% Tm^{3+}. Blue radiative decay of the regular lattice centre $(WO_4)^{-2}$ is also observed. No energy transfer exists between the W-O charge transfer state and $^1D_2$ level nor between $^1D_2$ and $^1G_4$; on the other side, it exists between W-O charge transfer state and the $^1G_4$ level. Because $LiIn_{1-x}Tm_x(WO_4)_2$ (x = 0, 0.5, 1, 5, and 10 at.%) phosphors exhibit intensive blue emission and under UV excitation, it is considered to be a new promising blue phosphor for field emission display application.

Acknowledgments

The authors wish to thank the help of O. Viraphong (ICMCB) and D. Tahtat (CRNA) for sample preparation, S. Boutarfaia (CRND) for the ATD analysis, H. Menari and S. Belhousse (UDTS) for performing the diffuse reflection and FTIR measurements, and Dr N. Souami (CRNA) for SEM images.

References

[1] X. Mateos, V. Petrov, J. Liu, et al., "Efficient 2-μm continuous-wave laser oscillation of Tm^{3+}: $Klu(WO_4)_2$," *IEEE Journal of Quantum Electronics*, vol. 42, no. 10, pp. 1008–1015, 2006.

[2] C. Cascales, A. M. Blas, M. Rico, V. Volkov, and C. Zaldo, "The optical spectroscopy of lanthanides R^{3+} in $(XO_4)_2$ (A = Li, Na; X = Mo, W) and $LiYb(MoO_4)_2$ multifunctional single crystals: relationship with the structural local disorder," *Optical Materials*, vol. 27, no. 11, pp. 1672–1680, 2005.

[3] G. Boulon, A. Brenier, L. Laversenne, et al., "Search of optimized trivalent ytterbium doped-inorganic crystals for laser applications," *Journal of Alloys and Compounds*, vol. 341, no. 1-2, pp. 2–7, 2002.

[4] H. Zhao, J. G. Wang, J. Li, et al., "Optical and thermal properties of crystalline Tb: $Klu(XO_4)_2$," *Materials Letters*, vol. 61, no. 11-12, pp. 2499–2501, 2007.

[5] A. García-Cortés, J. M. Cano-Torres, M. D. Serrano, et al., "Spectroscopy and lasing of Yb-doped $NaY(WO_4)_2$: tunable and femtosecond mode-locked laser operation," *IEEE Journal of Quantum Electronics*, vol. 43, no. 9, pp. 758–764, 2007.

[6] C. Tu, J. Li, Z. Zhu, Z. Chen, Y. Wang, and B. Wu, "Spectra and intensity parameters of Tm^{3+}: $KGd(WO_4)_2$ laser crystal," *Optics Communications*, vol. 227, no. 4–6, pp. 383–388, 2003.

[7] F. Song, L. Han, C. Zou, et al., "Upconversion blue emission dependence on the pump mechanism for Tm^{3+}-heavy-doped $NaY(WO_4)_2$ crystal," *Applied Physics B*, vol. 86, no. 4, pp. 653–660, 2007.

[8] X. Lu, Z. You, J. Li, et al., "Optical spectra of Tm^{3+} doped $NaBi(WO_4)_2$," *Optical Materials*, vol. 29, no. 7, pp. 849–853, 2007.

[9] J. M. Cano-Torres, X. Han, A. Garcìa-Cortés, et al., "Infrared spectroscopic and laser characterization of Tm in disordered double tungstates," *Materials Science and Engineering B*, vol. 146, no. 1–3, pp. 22–28, 2008.

[10] W. Guo, Y. Chen, Y. Lin, Z. Luo, X. Gong, and Y. Huang, "Spectroscopic properties and laser performance of Tm^{3+}-doped $NaLa(MoO_4)_2$ crystal," *Journal of Applied Physics*, vol. 103, no. 9, Article ID 093106, 2008.

[11] A. E. Borisevich, M. V. Korzhik, G. Yu. Drobychev, J. F. Cavaignac, and R. Chipaux, "New class of indium-containing room temperature inorganic scintillators," *Nuclear Instruments and Methods in Physics Research, Section A*, vol. 537, no. 1-2, pp. 228–231, 2005.

[12] M. Kobayashi, Y. Usuki, M. Ishii, and M. Itoh, "Significant increase in fast scintillation component from $PbWO_4$ by annealing," in *Nuclear Instruments and Methods in Physics Research, Section A*, vol. 537, no. 1-2, pp. 312–316, 2005.

[13] L. Macalik, J. Hanuza, D. Jaque, and J. Garcia Solé, "Spectroscopic characterisation of the Tm^{3+} doped $Kla(WO_4)_2$ single crystals," *Optical Materials*, vol. 28, no. 8-9, pp. 980–987, 2006.

[14] W. Ryba-Romanowski, S. Golab, I. Sokolska, et al., "Spectroscopic characterization of a Tm^{3+}: $SrGdGa_3O_7$ crystal," *Applied Physics B*, vol. 68, no. 2, pp. 199–205, 1999.

[15] S. W. Henderson and K. Ota, "Recent improvements in eyesafe, solid-state and coherent laser radar technology," *Review of Laser Engineering*, vol. 25, pp. 19–24, 1997.

[16] J. Su, F. Song, H. Tan, et al., "Phonon-assisted mechanisms and concentration dependence of Tm^{3+} blue upconversion luminescence in codoped $NaY(WO_4)_2$ crystals," *Journal of Physics D*, vol. 39, no. 10, pp. 2094–2099, 2006.

[17] J. Liao, B. Qiu, H. Wen, J. Chen, W. You, and L. Liu, "Synthesis process and luminescence properties of Tm^{3+} in AWO_4 (A = Ca, Sr, Ba) blue phosphors," *Journal of Alloys and Compounds*, vol. 487, no. 1-2, pp. 758–762, 2009.

[18] P. V. Klevtsov and R. F. Klevtsova, "Crystallographic investigation of a double tungstate, $LiFe(WO_4)_2$," *Soviet Physics: Crystallography*, vol. 15, no. 2, pp. 245–248, 1970.

[19] M. Maczka, K. Hermanowicz, P. E. Tomaszewski, M. Zawadzki, and J. Hanuza, "Synthesis and characterization of$NaLn(WO_4)_2$: Cr^{3+} nanoparticles," *Solid State Sciences*, vol. 10, no. 1, pp. 61–68, 2008.

[20] P. Kubelka and F. Munk, "Ein Beitrag zur Optik der Farbanstriche," *Z. Tech. Phys.*, vol. 12, p. 593, 1931.

[21] M. Maczka, J. Hanuza, and A. Pietraszko, "Vibrational and X-ray studies of the polymorphic forms of $sLiln(MoO_4)_2$," *Journal of Solid State Chemistry*, vol. 154, no. 2, pp. 498–506, 2000.

[22] M. Maczka, "Vibrational characteristics of the alkali metal-indium double molybdates $Mln(MoO_4)_2$ and Tungstates $Mln(MoO_4)_2$ (M = Li, Na, K, Cs)," *Journal of Solid State Chemistry*, vol. 129, no. 2, pp. 287–297, 1997.

[23] R. D. Shannon, "Revised effective ionic radii and systematic studies of interatomic distances in halides and chalcogenides," *Acta Crystallographica Section A*, vol. 32, no. 5, pp. 751–767, 1976.

[24] V. V. Fomichev and O. I. Kondratov, "Vibrational spectra of compounds with the wolframite structure," *Spectrochimica Acta Part A*, vol. 50, no. 6, pp. 1113–1120, 1994.

[25] M. C. Pujol, F. Güell, X. Mateos, et al., "Crystal growth and spectroscopic characterization of Tm^{3+}-doped $KYb(WO_4)_2$ single crystals," *Physical Review B*, vol. 66, no. 14, pp. 1443041–1443048, 2002.

[26] H. Zhang, X. Fu, S. Niu, and Q. Xin, "Blue emission of ZrO_2: Tm nanocrystals with different crystal structure under UV excitation," *Journal of Non-Crystalline Solids*, vol. 354, no. 14, pp. 1559–1563, 2008.

[27] L. Macalik, J. Hanuza, D. Jaque, and J. García Solé, "Spectroscopic characterisation of the Tm^{3+} doped $KLa(WO_4)_2$ single crystals," *Optical Materials*, vol. 28, no. 8-9, pp. 980–987, 2006.

[28] S. Shionoya and W. Yen, *Phosphor Handbook*, CRC Press, New York, NY, USA, 1999.